Barium stable isotopes in the global ocean: Tracer of Ba inputs and utilization

Yu-Te Hsieh[a,*] and Gideon M. Henderson[a]

[a]University of Oxford, Department of Earth Sciences, South Parks Road, Oxford, OX1 3AN, UK

Accepted manuscript for publication in Earth and Planetary Science Letters

Keywords: barium; seawater; barium isotopes; barium utilization; barium oceanic cycle; GEOTRACES.

Highlights:

1. Seawater $\delta^{138/134}$Ba values are strongly associated with the distribution of [Ba].
2. The upper ocean seawater [Ba] and $\delta^{138/134}$Ba integrate the ocean-basin scale signal.
3. Riverine input contributes light $\delta^{138/134}$Ba to the upper ocean seawater.
4. Upper-ocean $\delta^{138/134}$Ba shows correlations between Ba utilization and water mixing.
5. Deep-water $\delta^{138/134}$Ba is non-conservative during NADW-AABW mixing.

***Corresponding author: yu-te.hsieh@earth.ox.ac.uk**

Abstract

Barium has been used as a biogeochemical tracer for alkalinity, productivity, and riverine inputs in the ocean, but its oceanic cycle remains poorly constrained. Barium stable isotope measurements may improve the use of Ba as a tracer and better constrain the cycling of Ba, but data are only available in limited regions of the oceans. In this study, we present dissolved seawater Ba isotopic compositions in a sample collection spanning the North Atlantic, South Atlantic, North Pacific and Southern Oceans. Compiled global upper-ocean [Ba] data show a relatively constant [Ba] (35 ~ 45 nM) in the near-surface waters throughout the global ocean, with the exception of areas near river inputs or strong upwelling. The relatively uniform distribution of [Ba] in the upper ocean seawater indicates that Ba removal is slow relative to supply and mixing, and implies that near-surface Ba isotope values are controlled by basin-scale balances rather than by regional or short-term processes. Seawater Ba isotopic compositions show a large variation of $\delta^{138/134}$Ba values ranging from 0.24 to 0.65‰, and a tight relationship with [Ba]. This global relationship can be simply modeled assuming a primary deep Southern Ocean source for Ba to yield a maximum isotope fractionation of α = 1.00058 ± 0.00010 (α = $^{138/134}Ba_{seawater}/^{138/134}Ba_{particle}$). This suggested isotope fractionation during Ba removal from seawater is larger than implied by laboratory measurement during barite formation, suggesting additional fractionating phases or a two-stage fractionation process. Riverine input from the Rio de la Plata to the South Atlantic has a signature of $\delta^{138/134}$Ba = -0.06 ~ 0.11 ‰, which is too light to explain the heavy values (> 0.58 ‰) observed in the surface open ocean. Globally, the Ba isotope composition of the upper ocean waters is correlated with the fraction of Ba utilization at the basin scale (which varies from 15-70% at sites studied here). In the deep Atlantic Ocean, distinct

50 $\delta^{138/134}$Ba signals in the northern-sourced (≈0.45 ‰) and the southern-sourced water
51 (≈0.25 ‰) trace mixing and allow identification of non-conservative behavior of Ba,
52 reflecting additional inputs or sinks of Ba during transport (most likely addition from
53 sediment or hydrothermal). Ba isotopes may be useful to trace such inputs in the
54 present and past ocean.
55
56 **1. Introduction**
57 Barium is actively cycled in the oceans showing a broadly nutrient-like
58 distribution with surface depletion, deep-water enrichment, and an increase of
59 concentration in deep waters as they age from the North Atlantic to the Pacific.
60 Barium is not itself a primary nutrient, so this distribution is somewhat enigmatic. Its
61 marine geochemistry has been extensively investigated, partly to understand the
62 nutrient-like distribution (e.g. Chan et al., 1977; Dehairs et al., 1980), and partly for
63 the applications of Ba excess (e.g. Dymond et al., 1992; McManus et al., 1999) and
64 barite (e.g. Paytan et al., 1996a) as a tracer of past ocean productivity, or seawater
65 alkalinity and ocean circulation (e.g. Lea and Boyle, 1989; Jeandel et al., 1996; Rubin
66 et al., 2003). Due to the chemical similarities between Ba and Ra, Ba has also been
67 used for normalizing ^{226}Ra in seawater for studying large-scale ocean circulation (e.g.
68 Bacon and Edmond, 1972; Chan et al., 1976) and for Holocene marine carbonate
69 chronology (e.g. Paytan et al., 1996b; Staubwasser et al., 2004). Barium has also been
70 used as a water-mass tracer of riverine input to the coastal ocean by directly
71 measuring seawater [Ba] concentrations (Guay and Falkner, 1998) or Ba/Ca ratios in
72 corals (McCulloch et al., 2003) and foraminifera (Lea and Boyle, 1989).
73 Despite the uses of [Ba] or Ba/Ca ratios in the ocean, the processes controlling
74 Ba distribution and the role of biologically mediated barite formation remain

75 debatable. Decoupling between seawater [Ba] and [Si] in the surface ocean (Chan et
76 al., 1977; Jacquet et al., 2005), and between seawater [Ba] and alkalinity (Thomas et
77 al. 2011) suggests that the Ba oceanic cycle is not directly associated with either the
78 silica or carbonate cycle. Particulate studies have concluded that barite ($BaSO_4$)
79 formation and dissolution play an important role in Ba oceanic cycling (Dehairs et al.,
80 1980; Bishop, 1988), despite the fact that seawater is generally under-saturated with
81 respect to $BaSO_4$. Barite is primarily formed in the mesopelagic zone, where decay of
82 settling organic matter is thought to elevate the level of [Ba] in microenvironments to
83 reach the saturation point of $BaSO_4$ (e.g. Bishop, 1988; Monnin et al., 1999;
84 Ganeshram et al., 2003; Gonzalez-Muñoz et al., 2012). Marine bacteria (e.g.
85 Gonzalez-Muñoz et al., 2012) and Ba absorption onto other particles (e.g. metal
86 oxides, Sternberg et al., 2005) have also been identified as possible contributors to Ba
87 removal and barite formation in the upper ocean. The precise mechanisms and depth
88 of Ba removal and barite formation remain uncertain, however.
89 Stable Ba isotope fractionation has been investigated recently in experimental
90 materials and various minerals (von Allmen et al., 2010; Bottcher et al., 2012; van
91 Zuilen et al. 2016), igneous rocks (Miyazaki et al., 2014; Nan et al., 2015), soils
92 (Bullen and Chadwick, 2016), corals (Pretet et al., 2015) and seawater (Horner et al.,
93 2015; Cao et al., 2016; Bates et al., 2017). Von Allmen et al. (2010) discovered that
94 barite precipitation preferentially incorporates light Ba isotopes into sulphate minerals
95 and leaves heavy isotopes in the remaining solutions. Horner et al. (2015) found
96 substantial variations in Ba isotopic compositions between surface and deep waters,
97 and Bates et al. (2017) investigated the relationship of Ba isotopic compositions with
98 the ocean circulation in the Atlantic Ocean. Cao et al. (2016) also saw variations in
99 the South and East China Seas. These marine studies have shown that seawater Ba

isotope fractionation is not a localized signal but a tracer of large-scale Ba oceanic cycling and ocean circulation. Seawater measurements of Ba isotopes are limited, however, preventing assessment of their behavior at a global scale.

To improve understanding of Ba stable isotope fractionation in seawater and to characterize seawater Ba isotopic compositions in the global oceans, we have analyzed the dissolved Ba isotopic compositions in seawater samples collected from four major ocean basins in the North Atlantic, South Atlantic, North Pacific, and Southern Oceans (Fig. 1).

2. Samples and methods

2.1. Seawater sampling

Seawater samples analyzed in this study were collected from the North Atlantic (Hydrostation S, HydroS), the South Atlantic (UK-GEOTRACES, GA10W), the Southern Ocean (Bonus-GoodHope, GIPY4) and the North Pacific (ALOHA and SAFe stations) (Fig. 1a, Table 1). At each location, between 5 and 12 depths were analyzed. In the South Atlantic, four additional surface samples were analyzed, located from the measured profile towards the coast to the west, approaching the estuary of the Rio de la Plata. These samples cover a wide range of observed Ba concentrations (Fig. 1b). The North Atlantic depth profiles were collected from the Cruise 61183 (September 2011) at Hydrostation S; the South Atlantic samples during the UK-GEOTRACES cruise GA10W in the Argentine Basin (January 2012); the Southern Ocean seawater profile from the Weddell Gyre during the French Bonus-GoodHope expedition (March 2008); and the North Pacific samples from the ALOHA station during the HOE-PhoR-II cruise (September 2013). We also analyzed SAFe intercalibration samples (Johnson et al., 2007). The sampling methods used on these

cruises were similar (except for SAFe). Seawater samples were collected from the Niskin bottle rosette, immediately filtered with 0.45-micrometer Acropak cartridge filters, stored in pre-cleaned polypropylene bottles, and acidified to a pH of 1-2 with distilled HCl. For the SAFe samples, seawater samples were collected using the GeoFish and GO-Flo samplers for the surface and deep samples respectively, and filtered with 0.2-micrometer Poretics cartridge filters before acidification and storing.

2.2. Seawater Ba isotope method

The method of Ba purification used in this study is modified from the method described in Foster et al. (2004) and thus summarized only briefly here. Seawater (50 mL, ~ 250ng Ba) was weighed, and spiked with a ^{137}Ba-^{135}Ba double spike to allow correction for mass fractionation during chemical purification and instrument analysis (Text S1). A mixed spike-to-sample ratio of ~ 0.4 was targeted (ratio of total Ba) based on estimates of [Ba] at seawater sampling point. The double spike was calibrated by measuring the spike, the unspiked standard (NIST3104a), and a series of spike-standard mixtures in different proportions (Table S1). The double spike was also calibrated against the certified Ba concentration of NIST3104a (10.014 ± 0.036 mg/g, Lot No.070222) to determine the Ba concentration in samples. Three mL of a 0.9M Na_2CO_3 solution (with Ba previously removed by addition of Ca^{2+} to co-precipitate Ba with $CaCO_3$) was added to each spiked sample to co-precipitate Ba with $CaCO_3$. The precipitates were centrifuged, cleaned with H_2O and separated from the remaining seawater before being dissolved in 2 mL 3M HCl for column separation. AG50-X8 (200-400 mesh, 2 mL volume) was used to purify Ba from Ca, Mg, Sr, and REEs.

Ba isotope analyses were performed on a thermal ionization mass spectrometer (TIMS) Triton instrument at the University of Oxford. The sample loading method is adapted from Carlson et al. (2007); purified Ba samples/standards were dissolved in 2 μL of distilled 2M HCl, and loaded onto a single rhenium filament. A current of 0.68 A was continuously applied during the loading. Once the sample had dried on the filament, 2 μL of activator (a mixture of 50 mg Ta_2O_5 powder and 3mL 5% H_3PO_4) was loaded on top of the sample. During analysis, Ba-138, 137, 136, 135, 134, Ce-140 and La-139 ion beams were monitored in 7 Faraday cups simultaneously. In this study, the Ba-isotope data of samples are reported in the δ-notation (‰) ($\delta^{138/134}$Ba) relative to the Ba standard NIST3104a.

$$\delta^{138/134}Ba = (^{138/134}Ba_{sample} / {}^{138/134}Ba_{NIST} - 1) \times 1000 \quad (1)$$

Previous studies have reported Ba isotopic compositions variously as $\delta^{137/134}$Ba normalized to the Fluka $Ba(NO_3)_2$ standard (e.g. von Allmen et al., 2010; Pretet et al., 2015; Cao et al., 2016) or as $\delta^{138/134}$Ba normalized to NIST3104a (e.g. Horner et al. 2015). Horner et al. (2015) and Pretet et al. (2015) have both demonstrated that the differences between the Fluka and NIST Ba standards in their Ba isotopic compositions are within the analytical uncertainty. Therefore, $\delta^{137/134}$Ba can be simply converted to $\delta^{138/134}$Ba by directly multiplying by ≈1.33.

The long-term reproducibility of Ba isotope analysis in this study is generally better than 0.01‰ (2 standard deviations, n=11), based on repeated measurements of NIST3104a and one seawater sample from the North Atlantic, HyrdroS 10 m depth (Fig. S1). Incomplete separation of matrix elements from samples leads to somewhat larger uncertainty, between 0.01 and 0.05‰ (2 standard errors, n=500), which is

reported in this study. The overall procedural blank is between 0.7 and 1.2 ng of Ba, which was < 0.5% of the total Ba in seawater samples (≈250 ng)

3. Results

Water column profiles of dissolved [Ba] and $\delta^{138/134}$Ba from the five stations vary significantly and correspond to the distinct hydrographic setting of the locations (Fig. 1b, Fig. 2, Table 1). For comparison, macronutrient, salinity and temperature data are also provided in Table 1 and shown in Fig. S2. Ba concentrations show typical nutrient type profiles, similar to the profiles of other nutrients (Fig. S2). In Fig. 1b, we plot our dissolved [Ba] and [Si] data with the GEOSECS data from the Atlantic, Pacific and Southern Oceans (Chan et al. 1976; Chan et al. 1977; Bacon and Edmond 1972). The correlation between [Ba] and [Si] is similar to the trends observed in previous studies, except in areas where we detect riverine input from the Rio de la Plata (as seen by decreased salinity; Table 1) which are characterized by higher than expected [Ba] (Fig. 1b).

The depth profiles show that [Ba] generally has a consistent value in the top 300 m and increases with depth, ranging from 32.5 to 113.4 nM. Seawater $\delta^{138/134}$Ba composition is also stable within the top 300 m and decreases with depth from 0.65 to 0.24 $^{o}/_{oo}$ (Fig. 2). The North Atlantic and South Atlantic show similar [Ba] in the upper 200 m (≈44nM), but the South Atlantic has slightly higher $\delta^{138/134}$Ba (0.56-0.59‰) than the North Atlantic (0.52-0.54‰). The Southern Ocean [Ba] profile shows a relatively high concentration and homogeneous distribution from the surface water (84.8 nM) to the deep water (99.8 nM) and little variation in $\delta^{138/134}$Ba, ranging from 0.31‰ (surface) to 0.24‰ (deep). In the North Pacific (ALOHA and SAFe), [Ba] shows the largest gradient observed between the surface (25 m: 32.5 nM, the

lowest concentration observed in this study) and deep waters (1400 m: 113.4 nM, the highest concentration observed in this study). The profile of $\delta^{138/134}$Ba also shows the largest gradient from the surface (25 m: 0.65‰) to the deep water (1400 m: 0.26‰).

A plot of seawater $\delta^{138/134}$Ba ratios against 1/[Ba] (Fig 3), including data from Horner et al. (2015) and Bates et al. (2017), shows a strong correlation between seawater [Ba] and $\delta^{138/134}$Ba ratios, except for one anomalous data point at 498m from the SW Atlantic. This anomalous data point might indicate a unique regional process, but that would require more data and studies to identify.

The [Ba] and $\delta^{138/134}$Ba data from this study are consistent with those from previous studies. For example, they are similar to those of Horner et al. (2015) in the east basin of the South Atlantic (Fig. 2) and [Ba] is in good agreement with GEOSECS data (Chan et al., 1976; Chan et al., 1977; Hoppema et al., 2010) (Fig. S3).

4. Discussion

4.1. Ba in the near-surface ocean

Barium is a bio-intermediate element and has a nutrient-like distribution in the ocean. It is commonly compared to Si (e.g. Cao et al., 2016). [Ba] and $\delta^{138/134}$Ba show a similar distribution to [Si] and δ^{30}Si, with heavy isotopic compositions and low concentration in surface water due to removal associated with biology, and light isotopic values with high concentration in deep water due to particle remineralization (Fig. 2). In addition, Ba and Si isotopes both show meridional gradients in the deep Atlantic (e.g. de Souza et al., 2012), suggesting that ocean circulation plays an important role in deep-ocean Ba isotope composition.

Although the oceanic cycles of Ba and Si have been considered together, [Ba] in the global surface seawater is actually quite different from [Si]. We compile global surface seawater [Ba] data on a map in Fig. 4. Despite the general distribution of [Ba] being similar to [Si], i.e. low in pelagic oceans and high in regions with upwelled waters or riverine inputs, [Ba] is never depleted to the same extent as [Si] relative to deep waters and is relatively constant between 30 nM and 45 nM in the near-surface waters of the global ocean, with exceptions only in area of major riverine inputs (e.g. Arctic estuaries, [Ba] > 71 nM) and upwelling (e.g. Southern Ocean, [Ba] > 80 nM). In contrast, [Si] is much more depleted in pelagic surface seawater with [Si] values approaching 0 μM in many regions (e.g. Reynolds et al. 2006). The relative percentage of surface-water [Ba] (≈40 nM) to deep-water [Ba] (≈150 nM) is about 27%, but surface-water [Si] (≈1 μM) to deep-water [Si] (≈180 μM) is < 1% (Fig. 1). This demonstrates that Si has a more extreme removal than Ba in surface waters, which leads to a much greater variation of [Si] than [Ba] in the surface ocean.

The lack of complete removal of Ba from upper-ocean seawater reflects the fact that, unlike Si, it is not a primary limiting nutrient. In addition, barite, which is responsible for most downward flux of Ba, shows a better preservation in seawater, and hence a slower remineralization, than other nutrient carriers (e.g. opal, carbonate or organic matters) (Dehairs et al., 1980). This is expected to lead to a different regeneration history for [Ba] in deep waters compared to other nutrients, with a relatively slow increase in [Ba] and decrease in $\delta^{138/134}$Ba.

The relatively high and uniform concentration of Ba in the upper ocean indicates an important role for horizontal mixing and means that the open-ocean [Ba] is not controlled by local processes in surface water or in-situ regeneration in deep water. Instead, seawater Ba presents an integrated signal over a broad basin scale.

Open-ocean [Ba] is therefore unlikely to be suitable for studying local or short-term processes and should not be interpreted as only due to in-situ Ba isotope fractionation, or in one-dimensional models of vertical chemical cycling.

4.2. Global seawater Ba isotope fractionation and mixing models

The striking global correlation between [Ba] and $\delta^{138/134}$Ba (Fig. 3) indicates that the mechanism controlling Ba concentration and isotope ratio operates across all oceans. This correlation might be explained by three possible simple models: (1) Rayleigh fractionation in a closed system with decreasing [Ba]; (2) steady-state in an open system with continuous supply and removal of Ba; and (3) mixing between high and low [Ba] end-members. The true oceanic behavior of the Ba is likely to reflect a mixture of these three models, but it is instructive to consider the degree to which Ba behavior follows each simple model.

Closed-system Rayleigh fractionation follows the relationship:

$$\delta^{138/134}Ba_{sw} = \delta^{138/134}Ba_{sw\_0} + 1000\,(1/\alpha - 1)\ln(F) \quad (2)$$

And the open steady-state is described by the following equation:

$$\delta^{138/134}Ba_{sw} = \delta^{138/134}Ba_{sw\_0} - 1000\,(1/\alpha - 1) \times (1-F) \quad (3)$$

where $\delta^{138/134}Ba_{sw}$ and $\delta^{138/134}Ba_{sw\_0}$ denote the Ba isotope composition of the remaining seawater and the initial seawater, respectively. F is the fraction of remaining dissolved seawater Ba, which is given by $F = [Ba]/[Ba]_0$. The mass fractionation factor α is defined as $\alpha = {}^{138/134}Ba_{sw}/{}^{138/134}Ba_{particle}$ (α is reported or converted into per 4 amu in this paper), where ${}^{138/134}Ba_{sw}$ and ${}^{138/134}Ba_{particle}$ refer to the

274 $^{138/134}$Ba isotope ratios of seawater and the removed particulate phases (e.g. barite or
275 organic matter in surface seawater).
276
277 The two end-member mixing model is described by:
278 $$\delta^{138/134}Ba_{mix} = ([Ba]_A \times f \times \delta^{138/134}Ba_A + [Ba]_B \times (1-f) \times \delta^{138/134}Ba_B)/[Ba]_B \quad (4)$$
279
280 where mix, A and B refer to the components of mixed, and the A and B end-member
281 seawaters, respectively. The mixing ratio f is given by $f = M_A/M_{mix}$, with M_A and
282 M_{mix} denoting the masses of component A and of the mixture.
283 These simple models require assigning an isotope composition to the Ba that
284 mixes upwards to be removed from the near surface. Because there is significant
285 mixing of Ba within near-surface waters, it is inappropriate to consider local upward
286 mixing as the only source of Ba. Rather, the source of Ba is from upward mixing
287 across a broad region, from depths that are themselves experiencing mixing and
288 advection of waters with evolving Ba composition. To fully capture this complexity
289 would require incorporation of Ba and Ba isotopes into a spatially resolved ocean
290 model that mimics ocean circulation and the Ba cycle. A large-scale assessment of
291 the global pattern of Ba-isotope fractionation can, however, be made by considering
292 the evolution of Ba-isotopes from high-concentration deep-waters to the lower-
293 concentrations seen in the near-surface.
294 Previous studies of carbon, nutrients and trace elements have identified the
295 deep Southern Ocean as a critical source for return of chemical components from the
296 deep to shallower ocean (e.g. Sarmiento et al., 2004 for Si). These waters can
297 similarly be considered as the ultimate source of the Ba that mixes and upwells into
298 the near-surface ocean. The relatively high [Ba] of the Southern Ocean reflects

299 mixing of Ba from all oceans, and is fed back into all oceans to provide Ba which
300 ultimately mixes and upwells into the near-surface. At a global scale, these deep
301 Southern Ocean waters are an appropriate starting point for simple models of [Ba] and
302 Ba-isotope fractionation.

303 Average Southern Ocean waters below 2000 m have an initial composition of
304 [Ba] = 99.7 ± 0.8 nM (2 S.D.) and $\delta^{138/134}$Ba = 0.25 ± 0.02 ‰. (2 S.D.) All three
305 models are also fit to the observed composition of North Pacific surface ocean, which
306 has the lowest [Ba] (33.3 ± 1.6 nM, 2 S.D.) and highest $\delta^{138/134}$Ba (0.64 ± 0.03 ‰, 2
307 S.D.) yet observed in seawater, and can be considered the near-surface end point of
308 global Ba isotope fractionation. With these constraints, the open steady-state model
309 indicates a fractionation factor of 1.00058 ± 0.00010, and the closed Rayleigh model
310 a fractionation factor of 1.00035 ± 0.00010 (± 2 S.D. with uncertainties constrained
311 by uncertainty in end-members). The curves generated by these models, and by two-
312 end-member mixing, are shown relative to all global data in Fig. 3.

313 A closed Rayleigh model is unrealistic for Ba, given the influence of lateral
314 mixing and the long timescales of change. Such closed models are also thought to be
315 unsuitable for Si isotope in areas where [Si] is not fully depleted in the surface ocean
316 (Reynolds et al., 2006). Rayleigh models have also not been as successful as steady-
317 state models in explaining Ba-isotope observations in the ocean (Horner et al 2015;
318 Cao et al. 2016). The global $\delta^{138/134}$Ba data (Fig 3) support this view, indicating that
319 some data at mid [Ba] concentrations have $\delta^{138/134}$Ba too high to explain by a
320 Rayleigh model, which can only be explained by an open steady-state model.

321 The global Ba isotope data can all be explained by a combination of the open
322 steady-state model and ocean mixing. All data can therefore be fit by two processes;

323 mixing, and removal/addition of Ba with a single isotope fractionation of 1.00058 ±
324 0.00010.

325 Barite is a well-known carrier for Ba removal and remineralization (e.g.
326 Griffith and Paytan, 2012), and hence the best candidate as a major control on Ba
327 isotope fractionation in seawater. Laboratory precipitation of barite has indicated a
328 fractionation of 1.00032 ± 0.00005 (von Allmen et al., 2010). Seawater Ba-isotope
329 measurements in the Atlantic have been used to estimate a similar Ba isotope
330 fractionation of 1.00039 in the South Atlantic and of 1.00045 in the North Atlantic
331 based on the 1-D steady state model mixing from the sub-surface water (Horner et al.
332 2015; Bates et al. 2017). The larger fractionation required to fit the global data
333 suggests, however, that fractionation at the level observed during laboratory
334 precipitation of barite is insufficient to fully explain ocean behavior. Indeed, Cao et
335 al. (2016) measured co-existing particulate and dissolved Ba in the South China Sea
336 and observed still higher fractionation (α =1.00133), also suggesting that barite
337 fractionation reported from laboratory precipitation experiments is insufficient to
338 explain all Ba-isotope observations.

339 Seawater is undersaturated with respect to barite, so that precipitation of barite
340 requires pre-concentration of Ba, thought to occur in micro-environments rich in
341 organic material (e.g. Dehairs et al., 1980; Bishop et al., 1988; Sternberg et al., 2005).
342 This process requires two stages in the transport of Ba into barite; first from surface
343 seawater into organic matter, and then, at somewhat greater depth, from organic
344 matter into barite. If the formation of organic-matter favours the light isotope, as
345 would be expected, this could lead to a combined fractionation during Ba removal
346 larger than that for formation of barite alone. It is also possible that other processes
347 contribute to the observed fractionation, such as the involvement of bacteria in the

348 precipitation of natural marine barites (Gonzalez-Muñoz et al., 2012) or involvement
349 of other mineral phases (e.g. metal oxides; Sternberg et al., 2005)

350 The assumption made in this analysis, that the whole ocean can be considered
351 as having an input Ba composition equal to that of the deep Southern Ocean, is
352 simplistic, but likely to be more realistic than the assumption that waters immediately
353 below the surface at any location are the sole input to the near-surface at that location.
354 The latter, 1-D assumption, leads to calculation of lower and regionally variable
355 values for Ba isotope fractionation, which may underestimate the true value. Further
356 modeling, and analysis of $\delta^{138/134}$Ba in settling particles, will help refine assessment of
357 the isotope fractionation required to generate the striking global relationship observed
358 between Ba concentration and isotope composition, but analysis of this relationship at
359 a global scale suggests it is controlled by a combination of fractionation of 1.00058 ±
360 0.00010 during uptake, and mixing of high and low [Ba] waters in the global ocean.
361

362 **4.3. Riverine input to seawater Ba isotopes**

363 Riverine input is an important external source of Ba to the surface ocean
364 (Dehairs et al., 1980), with potential to influence surface-water compositions near
365 these inputs, and to control the global Ba isotope composition of the oceans on long
366 timescales. Cao et al. (2016) have measured isotopically light Ba, relative to typical
367 seawater, in eight rivers ($\delta^{138/134}$Ba = -0.1 to 0.4 ‰). These results suggest the use of
368 Ba isotopes as a tracer for riverine inputs in marginal seas.

369 Surface-water data from the SW Atlantic allow assessment of the $\delta^{138/134}$Ba
370 composition of another important river; the Rio de la Plata. We plot surface-water
371 data from the SW Atlantic against salinity to trace the Rio de la Plata outflow (Fig.
372 5a). These data show linear mixing between [Ba] and salinity with a relationship, [Ba]

373 = 208 (±60) - 4.7 (±1.9)×Salinity (Sal). Assuming riverine salinity of 0‰, this
374 indicates $[Ba]_{river}$ = 208 ± 60 nM. This concentration is a maximum estimate based on
375 the assumption of conservative mixing in the estuary, but is within the range of 100 to
376 500 nM observed in other rivers (Hanor and Chan 1977; Coffey et al., 1997; Joung
377 and Shiller, 2014; Cao et al., 2016). A two-component mixing model, similar to that
378 in Equation (4), is used to calculate the riverine $\delta^{138/134}Ba_{riv}$ (Fig. 5b):
379 $\delta^{138/134}Ba_{mix} = ([Ba]_{riv}\times f\times\delta^{138/134}Ba_{riv} + [Ba]_{sw}\times(1-f)\times\delta^{138/134}Ba_{sw})/[Ba]_{mix}$
380 (5)
381 where *mix*, *riv*, and *sw* refer to mixed, riverine, and seawater values respectively; f is
382 the fraction of riverine input between salinity 0 ‰ (f = 1) and 35 ‰ (f = 0) during
383 mixing. Considering the large uncertainty of $[Ba]_{riv}$ from 148nM to 268nM, the
384 mixing curves indicate $\delta^{138/134}Ba_{riv}$ values between -0.06 and 0.11 ‰ for the Ba
385 released to the open ocean by the Rio de la Plata, within the range of previously
386 measured riverine $\delta^{138/134}$Ba values (-0.1 ~ 0.4 ‰) (Cao et al., 2016). Such
387 extrapolation does not constrain the pure riverine composition because there is a
388 possibility of isotope fractionation occurring during non-conservative mixing of Ba
389 released from riverine particles, but it does provide information about the Ba flux and
390 isotope composition of input to the open ocean after any estuarine alteration. This
391 analysis also assumes that the Ba anomalies seen in SW Atlantic surface water relate
392 to the Rio de la Plata, rather than any other source (such as submarine groundwater
393 discharge).
394 The light riverine $\delta^{138/134}$Ba values observed previously, and now in the Rio de
395 la Plata, indicate that heavy $\delta^{138/134}$Ba values (0.56-0.59‰) observed in the surface
396 South Atlantic cannot be explained by riverine input. This observation is consistent
397 with the fact that riverine input is less than 18% of the Ba input to the surface ocean

398 (e.g. Wolgemuth and Broecker, 1970; Dehairs et al., 1980) with internal ocean
399 cycling dominating the supply.

400 This study agrees with previous work in indicating that riverine $\delta^{138/134}$Ba
401 values are isotopically light, supporting the use of Ba isotopes as a tracer of riverine
402 inputs in coastal waters.

403

404 **4.4. Ocean-basin Ba utilization**

405 For nutrient elements, the term utilization describes the fraction of the nutrient
406 removed in surface waters, relative to the initial amount upwelled to the surface.
407 Although Ba removal is not dominated by direct biological utilization and barite
408 precipitation tends to happen in a deeper depth (> 100m) of the upper ocean, we adopt
409 the same term – utilization – to describe the removal of Ba from upper ocean waters
410 (< 400 m). As discussed above, open-ocean Ba in upper ocean waters is strongly
411 impacted by lateral mixing, so any measure of Ba utilization will be for a broad and
412 basin-scale region rather than due to local removal. The strong relationship observed
413 in the global oceans between [Ba] and $\delta^{138/134}$Ba indicates that increasing Ba
414 utilization will lead to progressively higher $\delta^{138/134}$Ba in the upper ocean waters. Ba
415 isotopes may therefore provide information about Ba utilization at a basin scale.

416 Assuming, as in Section 4.2, that the ocean-scale supply of Ba originates from
417 the deep Southern Ocean, we can assess basin-scale Ba utilization (= 1 – ([Ba]/$[Ba]_0$)
418 by comparing seawater [Ba] values from < 400 m at each location to the average
419 concentration of Ba from the deep Southern Ocean (> 2000 m; $[Ba]_0$ = 99.7 nM). This
420 results in Ba utilization values, relative to the ultimate Southern Ocean source, of
421 ≈70% for the North Pacific, ≈55% for the South Atlantic and the North Atlantic, and
422 only <15% for the Southern Ocean (Fig. 6). This pattern of utilization is broadly

423 reflected in upper ocean [Ba] values which are slightly higher [Ba] (≈45 nM) in the
424 Atlantic than the North Pacific (≈35 nM) (Fig. 4). The high utilization of the North
425 Pacific may result from slower upward mixing, allowing more time for biological
426 consumption in the upper ocean, and/or by increased removal by productivity.
427 Previous studies suggest that the North Pacific subtropical gyre has weak vertical
428 mixing from intermediate waters to the upper ocean (e.g. Emery and Dewar, 1982),
429 which suggests that lower supply may be the dominant influence.

430 Barium utilization defined relative to the deep Southern Ocean value in this
431 way can be deduced simply from the upper ocean [Ba] for the modern ocean, so
432 $\delta^{138/134}$Ba may not provide significant new information. The upper ocean $\delta^{138/134}$Ba
433 may, however, be more readily recorded in paleo-archives, such as corals, than
434 seawater Ba concentrations, to allow assessment of past Ba utilization.

435

436 **4.5. Ba isotope in deepwaters: The Atlantic Ocean**

437 Data for [Ba] and $\delta^{138/134}$Ba in the Atlantic Ocean allow consideration of the
438 controls on Ba cycling in the deep-ocean, and the potential for use of Ba isotopes as a
439 tracer of water-mass or of Ba inputs. The distribution of [Ba] broadly follows the
440 major water masses in the Atlantic Ocean (Fig. 7), as does the distribution of
441 $\delta^{138/134}$Ba. Deep-water [Ba] and Ba-isotopes reflect the value inherited as waters leave
442 the surface (i.e. preformed Ba), but are also influenced by addition of Ba through
443 regeneration of biogenic particles, sediment dissolution and hydrothermal inputs. The
444 extent to which such additions alter a water mass composition as it ages will control
445 whether $\delta^{138/134}$Ba is a more powerful tracer of water-mass during mixing and
446 advection, or of the inputs of Ba to seawater

To assess controls on deep-water Ba composition, and the degree to which Ba is a conservative tracer in the deep ocean, we start by constraining southern and northern end-member Ba concentrations for the Atlantic. A plot of [Ba] versus salinity below 2000 m shows a linear relationship with [Ba] = 5413.3 – 153.2 × Sal. (R^2 = 0.88) (Fig. 8a). Antarctic Bottom Water (AABW) and North Atlantic Deep Water (NADW) are characterized by distinct salinity values of 34.66 ‰ and 35.00 ‰ respectively (Emery and Meincke, 1986), and these values can be used, with the observed linear relationship, to assess [Ba] in AABW and NADW as 103 ± 10 nM and 51± 5 nM respectively. Our estimates are consistent with previous studies (e.g. Chan et al., 1977; Hoppema et al., 2010) that have indicated [Ba] = 100 - 106 nM in deep waters sourced in the Southern Ocean, and [Ba] = 48 - 52 nM in North Atlantic Deep Water.

End-member values for deep-water [Ba], coupled to observations of the relationship between [Ba] and $\delta^{138/134}$Ba in this study, allow end-member value for $\delta^{138/134}$Ba to be assigned to Antarctic Bottom Water (AABW) and North Atlantic Deep Water (NADW); of ≈0.25 ‰ and ≈0.45 ‰ respectively. These results are consistent with the estimates in a recent study (Bates et al., 2017) (Fig. 8b).

If Ba behaves entirely conservatively in the deep-ocean, all compositions during flow and mixing of these two water masses should fall on a straight line between the defined end-members in a plot of $\delta^{138/134}$Ba versus 1/[Ba]. Bates et al. (2017) considered the behavior of Ba as “near-conservative” in the deep Atlantic, because most available deep-water data were distributed around this straight mixing line. Bates et al., however, excluded one data point from the deep North Atlantic that deviated from the conservative-mixing behaviour because of potential influence from additional Ba inputs. Combining the data from Bates et al. (2017) and this study (Fig.

8b) shows that such a deviation is not a single anomaly. These deviations can also be seen in the South Atlantic below 4000 m (+ 0.05 ‰ offset) and between 2000 and 3000 m (+ 0.08 ‰ offset) (Fig. 8b).

Deviations of deep-water $\delta^{138/134}$Ba from the mixing line indicate a non-conservative component of Ba behavior, superimposed on the strong water-mass control on composition. This non-conservative behavior might be due to addition of Ba from settling particles, sediments, or hydrothermal activity, or due to removal by scavenging onto settling particles or at the seafloor. Addition of Ba from settling particles is unlikely to generate deviations from the mixing line because it involves the same process that leads to the initial isotopic differences between the end-members. Addition from sediment is more likely, because sedimentary fluxes of Ba represent about 15% of the total input to the deep ocean below 3000 m (Paytan and Kastner, 1996) and sediments contain pools of Ba in carbonates, barite, organic matter, opal, metal oxides, terrestrial silicates and other detrital material (Gonneea and Paytan, 2006), each of which may have different isotopic compositions. Metal oxide formation in sediments could also remove Ba from deep waters, with a Ba isotope fractionation value which is presently unknown. Mid-ocean-ridge vent fluids are known to be enriched with [Ba] by a factor of ≈80-420 relative to deep seawater (e.g. von Damm et al., 1985). Such enrichment in the hydrothermal processes may reflect a different isotope effect than sediments or settling particles.

This analysis of deep-water compositions demonstrates the potential for $\delta^{138/134}$Ba to provide information about deep water mass mixing and the cycling of Ba, and indicates the presence of non-conservative behavior, most likely due to addition of Ba from sediments or hydrothermal systems in the deep-ocean.

5. Conclusions

We report dissolved Ba concentrations and Ba isotopic compositions in seawaters from the North Atlantic, South Atlantic, North Pacific, and Southern Oceans. Surface seawater [Ba] data from these sites and from earlier work show relatively uniform distribution of [Ba] in the upper ocean seawater, except in regions of riverine Ba input or strong upwelling. This uniform composition reflects the relatively low level of depletion of [Ba] in the upper ocean compared with that for the nutrients, and the consequent importance of lateral mixing. The upper ocean water Ba isotope values therefore reflect basin-scale balances rather than local or short-term processes.

A tight correlation between [Ba] and $\delta^{138/134}$Ba is observed in the global ocean, and can be explained by a removal/addition process with an isotope fractionation factor of $\alpha = 1.00058 \pm 0.00010$ and by mixing between the deep Southern Ocean and global upper ocean waters. This fractionation factor is an upper-limit for the average global value and represents the net processes of Ba removal and addition. It is likely that the oceanic fractionation is larger than that assessed from 1D assessment of upward mixing Ba, and from inorganic barite growth in the laboratory.

Riverine input from the Rio de la Plata to the South Atlantic shows a lighter $\delta^{138/134}$Ba signature than the open ocean surface values, suggesting that Ba riverine input to the surface ocean is insignificant compared to the fluxes of Ba from internal cycling. Away from riverine input, global surface water Ba isotope composition is correlated with the fraction of Ba utilization at the basin scale.

In the deep Atlantic, non-conservative behaviour of Ba is suggested from combined [Ba] and $\delta^{138/134}$Ba data. Input from sediments or hydrothermal activity might be responsible for this non-conservative behaviour, and isotope data for these

sources would enable their significance to be assessed and the oceanic cycling of Ba better understood.

Acknowledgments

We thank C. Hayes, M. Boye, G. Smith, and K. Bruland for sampling seawater and sharing the samples for this study. We are grateful to the crews and scientists on the UK-GEOTRACES cruise (GA10W), the French Bonus-Good Hope cruise (GIPY4), and the HOE-PhoR-II cruise for their assistances with the sampling. We would like to thank Alan Shiller for providing seawater [Ba] data from the US-GEOTRACES cruises (GA03 and GP16) for use in Figure 4. We would also like to thank S.N. Burgess for preparing the Ba double spike, P. Bonnand for discussion of TIMS methods, and L. Bridgestock and D. Porcelli for discussions of Ba isotopes in oceanic cycling. Greg de Souza and other three anonymous reviewers are appreciated for their valuable comments to improve this paper.

References

Bacon, M.P., Edmond, J.M., 1972. Barium at GEOSECS III in the southeast Pacific. Earth Planet. Sci. Lett. 16, 66-74. doi:10.1016/0012-821X(72)90237-3

Bates, S.L., Hendry, K.R., Pryer, H.V., Kinsley, C.W., Pyle, K.M., Woodward, E.M.S., Horner, T.J., 2017. Barium isotopes reveal role of ocean circulation on barium cycling in the Atlantic. Geochim. Cosmochim. Acta 204, 286-299. https://doi.org/10.1016/j.gca.2017.01.043

Bishop, J.K.B., 1988. The barite-opal-organic carbon association in oceanic particulate matter. Nature 332, 341-343. doi:10.1038/332341a0

546 Bottcher, M.E., Geprags, P., Neubert, N., von Allmen, K., Pretet, C., Samankassou,
547 E., Nagler, T.F., 2012. Barium isotope fractionation during experimental formation
548 of the double carbonate $BaMn(CO_3)_2$ at ambient temperature. Isot. Environ. Health
549 Stud. 48, 457-463. doi:10.1080/10256016.2012.673489
550 Bullen, T., Chadwick, O., 2016. Ca, Sr and Ba stable isotopes reveal the fate of soil
551 nutrients along a tropical climosequence in Hawaii. Chem. Geol. 422, 25-45.
552 http://dx.doi.org/10.1016/j.chemgeo.2015.12.008
553 Cao, Z., Sibert, C., Hathorne, E.C., Dai, M., Frank, M. 2016. Constraining the oceanic
554 barium cycle with table barium isotopes. Earth Planet. Sci. Lett. 434, 1-9.
555 http://dx.doi.org/10.1016/j.epsl.2015.11.017
556 Carlson, R.W., Boyet, M., Horan, M., 2007. Chondrite barium, neodymium, and
557 samarium isotopic heterogeneity and early earth differentiation. Science 316,
558 1175-1178. doi:10.1126/science.1140189
559 Chan, L.H., Edmond, J.M., Stallard, R.F., Broecker, W.S., Chung, Y.C., Weiss, R.F.,
560 Ku, T.L., 1976. Radium and barium at GEOSECS stations in the Atlantic and
561 Pacific. Earth Planet. Sci. Lett. 32, 258-267. doi:10.1016/0012-821X(76)90066-2
562 Chan, L.H., Drummond, D., Edmond, J.M., Grant, B., 1977. On the barium data from
563 the Atlantic GEOSECS expedition. Deep-Sea Res. 24, 613-649. doi:10.1016/0146-
564 6291(77)90505-7
565 Coffey, M., Dehairs, F., Collette, O., Luther, G., Church, T., Jickells, T., 1997. The
566 behaviour of dissolved barium in estuaries. Est. Coastal Shelf Sci. 45, 113-121.
567 doi:10.1006/ecss.1996.0157
568 de Souza, G.F., Reynolds, B.C., Rijckli, J., Frank, M., Saito, M.A. Gerringa, L.J.A.,
569 Bourdon, B., 2012. Southern Ocean control of silicon stable isotope distribution in
570 the deep Atlantic Ocean. Glob. Biogeochem. Cyc. 26. doi: 10.1029/2011gb004141

571 Dehairs, F., Chesselet, R., Jedwab, J., 1980. Discrete suspended particles of barite and
572 the barium cycle in the open ocean. Earth Planet. Sci. Lett. 49, 528-550.
573 doi:10.1016/0012-821X(80)90094-1
574 Dymond, J., Suess, E., Lyle, M., 1992. Barium in deep-sea sediment: A geochemical
575 proxy for paleoproductivity. Paleoceanography 7, 163-181.
576 doi:10.1029/92PA00181
577 Emery, W.J., Dewar, J.S., 1982. Mean Temperature-Salinity, Salinity-Depth and
578 Temperature-Depth Curves for the North-Atlantic and the North Pacific. Progress
579 in Oceanography 11, 219-256. doi:10.1016/0079-6611(82)90015-5
580 Emery, W.J., Meincke, J., 1986. Global water masses: summary and review.
581 Oceanologica Acta 9, 383-391.
582 Foster, D.A., Staubwasser, M., Henderson, G.M., 2004. 226Ra and Ba concentrations
583 in the Ross Sea measured with multicollector ICP mass spectrometry. Mar. Chem.
584 87, 59-71. doi:10.1016/j.marchem.2004.02.003
585 Ganeshram, R.S., Francois, R., Commeau, J., Brown-Leger, S.L., 2003. An
586 experimental investigation of barite formation in seawater. Geochim. Cosmochim.
587 Acta 67, 2599-2605. https://doi.org/10.106/S0016-7037(03)00164-9
588 Gonneea, M.E., Paytan, A., 2006. Phase associations of barium in marine sediments.
589 Mar. Chem. 100, 124-135. http://dx.doi.org/10.1016/j.marchem.2005.12.003
590 Gonzalez-Muñoz, M.T., Martinez-Ruiz, F., Morcillo, F., Martin-Ramos, J.D., Paytan,
591 A., 2012. Precipitation of barite by marine bacteria: A possible mechanism for
592 marine barite formation. Geology 40, 675-678. doi: 10.1130/G33006.1
593 Griffith, E.M., Paytan, A., 2012. Barite in the ocean – occurrence, geochemistry and
594 palaeoceanographic applications. Sedimentology 59, 1817-1835. doi:
595 10.1111/j.1365-3091.2012.01327.x

596 Guay, C.K., Falkner, K.K. 1998. Barium as a tracer of Arctic halocline and river
597 waters. Deep-Sea Res. II 44, 1543-1569. doi:10.1016/S0967-0645(97)00066-0
598 Hanor, J.S., Chan, L.H., 1977. Non-conservative behaviour of barium during mixing
599 of Mississippi River and Gulf of Mexico waters. Earth Planet. Sci. Lett. 37, 242-
600 250. doi:10.1016/0012-821X(77)90169-8
601 Hoppema, M., Dehairs, F., Navez, J., Monnin, C., Jeandel, C., Fahrbach, E., de Baar,
602 H.J.W., 2010. Distribution of barium in the Weddell Gyre: Impact of circulation
603 and biogeochemical processes. Mar. Chem. 122, 118-129.
604 doi:10.1016/j.marchem.2010.07.005
605 Horner, T.J., Kinsley, C., Nielsen, S.G., 2015. Barium-isotopic fractionation in
606 seawater mediated by barite cycling and oceanic circulation. Earth Planet. Sci.
607 Lett. 430, 511-522. doi: 10.1016/j.epsl.2015.07.027
608 Jacquet, S.H.M., Dehairs, F., Cardinal, D., Navez, J., Delille, B., 2005. Barium
609 distribution across the Southern Ocean frontal system in the Cozet-Kerguelen
610 Basin. Mar. Chem. 95, 149-162. http://dx.doi.org/10.1016/j.marchem.2004.09.002
611 Jeandel, C., Dupré, B., Lebaron, G., Monnin, C., Minster, J.-F., 1996. Longitudinal
612 distributions of dissolved barium, silica and alkalinity in the western and southern
613 Indian Ocean. Deep-Sea Res. I 43, 1-31. doi:10.1016/0967-0637(95)00098-4
614 Johnson, K.S., et al., 2007. Developing standards for dissolved iron in seawater. EOS
615 Trans. AGU 88, 131-132. doi: 10.1029/2007EO110003
616 Joung, D., Shiller, A.M., 2014. Dissolved barium behavior in Louisiana Shelf waters
617 affected by the Mississippi/Atchafalaya River mixing zone. Geochim. Cosmochim.
618 Acta 141, 303-313. http://dx.doi.org/10.1016/j.gca.2014.06.021
619 Lea, D., Boyle, E., 1989. Barium content of benthic foraminifera controlled by
620 bottom-water composition. Nature 338, 751-753. doi:10.1038/338751a0

621 Mawji. E., et al., 2015. The GEOTRACES intermediate data product 2014. Mar.
622 Chem. 177, 1-8. http://dx.doi.org/10.1016/j.marchem.2015.04.005
623 McCulloch, M., Fallon, S., Wyndham, T., Hendy, E., Lough, J., Barnes, D., 2003.
624 Coral record of increased sediment flux to the inner Great Barrier Reef since
625 European settlement. Nature 421, 727-730. doi:10.1038/nature01361
626 McManus, J., Berelson, W.M., Hammond, D.E., Klinkhammer, G.P., 1999. Barium
627 cycling in the North Pacfic: implications for the utility of Ba as a paleoproductivity
628 and paleoalkalinity proxy. Paleoceanography 14, 53-61.
629 doi:10.1029/1998PA900007
630 Miyazaki, T., Kimura, J.I., Chang, Q., 2014. Analysis of stable isotope ratios of Ba by
631 double-spike standard-sample bracketing using multiple-collector inductively
632 coupled plasma mass spectrometry. J. Anal. At. Spectrom. 29, 483-490.
633 doi:10.1039/c3ja50311a
634 Monnin, C., Jeandel, C., Cattaldo, T., Dehairs, F., 1999. The marine barite saturation
635 state of the world's oceans. Mar. Chem. 65, 253-261. doi:10.1016/S0304-
636 4203(99)00016-X
637 Nan, X., Wu, F., Zhang, Z., Hou, Z., Huang, F., Yu, H., 2015. High-precision barium
638 isotope measurements by MC-ICP-MS. J. Anal. At. Spectrom. 30, 2307-2315.
639 doi:10.1039/C5JA00166H
640 Paytan, A., Kastner, M., Chavez, F.P, 1996a. Glacial to interglacial fluctuations in
641 productivity in the Equatorial Pacific as indicated by marine barite. Science 274,
642 1355-1357. doi: 10.1126/science.274.5291.1355
643 Paytan, A., Moore, W.S., Kastner, M., 1996b. Sedimentation rate as determined by
644 226Ra activity in marine barite. Geochim. Cosmochim. Acta 60, 4313-4319.
645 https://doi.org/10.1016/S0016-7073(96)00267-0

646 Paytan, A., Kastner, M., 1996. Benthic Ba fluxes in the central Equatorial Pacific,
647 implications for the oceanic Ba cycle. Earth Planet. Sci. Lett. 142, 439-450.
648 doi:10.1016/0012-821X(96)00120-3
649 Pretet, C., van Zuilen, K., Nägler, T.F., Reynaud, S., 2015. Constrains on barium
650 isotope fractionation during aragonite precipitation by corals. The journal of
651 International Association of Sedimentologists 1, 118-129. doi: 10.1002/dep2.8
652 Reynolds, B.C., Frank, M., Halliday, A.N., 2006. Silicon isotope fractionation during
653 nutrient utilization in the North Pacific. Earth Planet. Sci. Lett. 244, 431-443.
654 http://dx.doi.org/10.1016/j.epsl.2006.02.002
655 Roeske, T., Bauch, D., Rutgers V.D. Loeff, M., Rabe, B., 2012. Utility of dissolved
656 barium in distinguishing North American from Eurasian runoff in the Arctic
657 Ocean. Mar. Chem. 132, 1-14.
658 Rubin, S.I., King., S.L., Jahnke, R.A., Froelich, P.N., 2003. Benthic barium and
659 alkalinity fluxes: Is Ba an oceanic paleo-alkalinity proxy for glacial atmospheric
660 CO_2? Geophys. Res. Lett. 30, 1885. doi:10.1029/2003GL017339
661 Singh, S.P., Singh, S.K., Bhushan, R., 2013. Internal cycling of dissolved barium in
662 water column of the Bay of Bengal. Mar. Chem. 154, 12-23.
663 http://dx.doi.org/10.1016/j.marchem.2013.04.013
664 Sarmiento, J.L., Gruber, N., Brzezinski, M.A., Dunne, J.P., 2004. High-latitude
665 controls of thermocline nutrients and low latitude biological productivity. Nature
666 427, 56-60.
667 Staubwasser, M., Henderson, G.M., Berkman, P.A., Hall, B.L., 2004. Ba, Ra. Th, and
668 U in marine mollusc shells and the potential of 226Ra/Ba dating of Holocene
669 marine carbonate shells. Geochim. Cosmochim. Acta 68, 89-100.
670 http://dx.doi.org/10.1016/S0016-7037(03)00279-5

671 Sternberg, E., Tang, D., Ho, T.-Y., Jeandel, C., Morel, F.M.M., 2005. Barium uptake
672 and adsorption in diatoms. Geochim. Cosmochim. Acta 69, 2745-2752.
673 http://dx.doi.org/10.1016/j.gca.2004.11.026
674 Thomas, H., Shadwich, E., Dehairs, F., Lansard, B., Mucci, A., Navez, J., Gratton, Y.,
675 Prowe, F., Chierici, M., Fransson, A., Papakyriakou, T.N., Sternberg. E., Miller,
676 L.A., Tremblay, J.-E. 2011. Barium and carbon fluxes in the Canadian Arctic
677 Archipelago. J. Geophys. Res. 116, C00G08. doi: 10.1029/2011JC007120
678 van Zuilen, K., Müller, T., Nägler, T.F., Dietzel, M., Küsters, T., 2016. Experimental
679 determination of barium isotope fractionation during diffusion and adsorption
680 processes at low temperatures. Geochim. Cosmochim. Acta 186, 226-241.
681 http://dx.doi.org/10.1016/j.gca.2016.04.049
682 von Allmen, K., Bottcher, M.E., Samankassou, E., Nagler, T.F., 2010. Barium isotope
683 fractionation in the global barium cycle: First evidence from barium minerals and
684 precipitation experiments. Chem. Geol. 277, 70-77.
685 doi:10.1016/j.chemgeo.2010.07.011
686 von Damm, K.L., Edmond, J.M., Measures, C.I., Grant, B., 1985. Chemistry of
687 submarine hydrothermal solutions at Guaymas Basin, Gulf of California. Geochim.
688 Cosmochim. Acta 49, 2221-2237. doi:10.1016/0016-7037(85)90223-6
689

690 **Figure and Table Captions**

691 **Table 1** Seawater sample information, temperature, salinity, Ba concentration, and Ba
692 isotope composition.
693

694 **Figure 1** Map of sampling locations and the distribution of dissolved [Ba] and [Si] in
695 global seawater. (a) The station symbols and data are colour coded consistently for

each station throughout this paper. The data for GA10E (Stn6) are taken from Horner et al. (2015). (b) The yellow circles are samples that were collected along the GA10W cruise from Stn20 towards the Rio de la Plata in the SW Atlantic. Latitudes and longitudes are in Table 1. The [Ba] and [Si] concentrations from the GEOSECS Atlantic, Pacific and Southern Ocean dataset are shown in grey open circles (from https://odv.awi.de/en/data/ocean/geosecs/).

Figure 2 Depth profiles of **(a)** Ba concentrations and **(b)** Ba isotope compositions. The error bars of the data are 2 standard errors (2 S.E.), and are within the size of the symbols for [Ba]. The data for the SE Atlantic (Stn6) are taken from Horner et al. (2015).

Figure 3 Ba isotope compositions versus 1/[Ba] for all seawater samples from this study, Horner et al. (2015) and Bates et al. (2017). The data are fitted with three curves generated by a steady-state (open) model, a Rayleigh fractionation (closed) model and a mixing model, each constrained using an initial composition equal to the average value in the deep Southern Ocean, and a final value equal to the surface values in the Pacific Ocean.

Figure 4 Global surface seawater [Ba] map (< 200m). Data sources are from the GEOSECS (Chan et al. 1976; Chan et al. 1977; Bacon and Edmond 1972), the GEOTRACES Intermediate Data Product 2014 (Cruises: GIPY4: Hoppema et al. 2010; GIPY5: data courtesy of T. Roeske and M. Rutgers van der Loeff; GIPY11: Roeske et al. 2012; GA02: data courtesy of A. Vilela and J.M. Godoy), and other GEOTRACES Cruises (GA03 and GP16 data courtesy of A. Shiller, and GA10:

721 Horner et al. 2015 and this study) for the global oceans, and Singh et al. (2013) for
722 Bay of Bengal, and Cao et al. (2016) for the South and East China Seas.
723
724 **Figure 5** Ba concentrations and isotopic compositions in the surface samples with
725 riverine input from the Rio de la Plata in the SW Atlantic. **(a)** Ba concentration versus
726 salinity shows evidence for mixing between seawater and riverine input indicating a
727 [Ba] = 208 ± 60 nM in the riverine input at salinity of 0 ‰. **(b)** Seawater $\delta^{138/134}$Ba
728 versus salinity. The solid and dashed lines show the two end-member mixing curve
729 between seawater (salinity at 35 ‰) and riverine input (salinity at 0 ‰) with a range
730 of estimate of river [Ba] from 148 nM to 268 nM and predicted $\delta^{138/134}$Ba from -0.06
731 to 0.11 ‰. The range of observed global riverine $\delta^{138/134}$Ba from eight rivers is
732 labeled in light blue (data from Cao et al. 2016).
733
734 **Figure 6** Seawater Ba isotopic compositions and the relative basin-scale Ba
735 utilization relative to the composition of the deep Southern Ocean. The relative ocean-
736 basin-scale Ba utilization is calculated by normalizing surface seawater [Ba] (< 400m)
737 to the average [Ba] (99.7 nM) in the deep Southern Ocean (> 2000m).
738
739 **Figure 7** Seawater [Ba] and $\delta^{138/134}$Ba profiles in a N-S Atlantic section. The
740 dissolved [Ba] data are from the GEOTRACES Intermediate Data Product 2014
741 (Mawji et al., 2015) and the GEOSECS Ba dataset (Fig. 1b). Seawater $\delta^{138/134}$Ba
742 profiles are shown for the North Atlantic, South Atlantic and Southern Oceans (from
743 this study).
744

Figure 8 Seawater [Ba] and $\delta^{138/134}$Ba below 2000 m in the Atlantic. **(a)** The linear regression of [Ba] and salinity in the deep Atlantic Ocean; end-member salinity values are 35.00 and 34.66 ‰ in NADW and AABW respectively (Emery and Meincke, 1986), suggesting [Ba] of 51 ± 5 nM and 103 ± 10 nM in NADW and AABW respectively. **(b)** Deep-water $\delta^{138/134}$Ba versus 1/[Ba]. The end-member [Ba] concentrations in NADW and AABW are labeled with blue and red lines respectively, which indicate that NADW has a $\delta^{138/134}$Ba value of 0.45 ‰ and AABW has a $\delta^{138/134}$Ba value of 0.25 ‰. Deep-water $\delta^{138/134}$Ba and [Ba] in the South Atlantic show non-conservative mixing during the N-S Atlantic water transport as highlighted by purple arrows and circles. These deviations show $\delta^{138/134}$Ba offsets of 0.05 ~ 0.14 ‰ from the mixing line in deep waters. The SE Atlantic data (labeled in gray) and the NE and NW Atlantic data (labeled in light blue) are from Horner et al. (2015) and Bates et al. (2017).

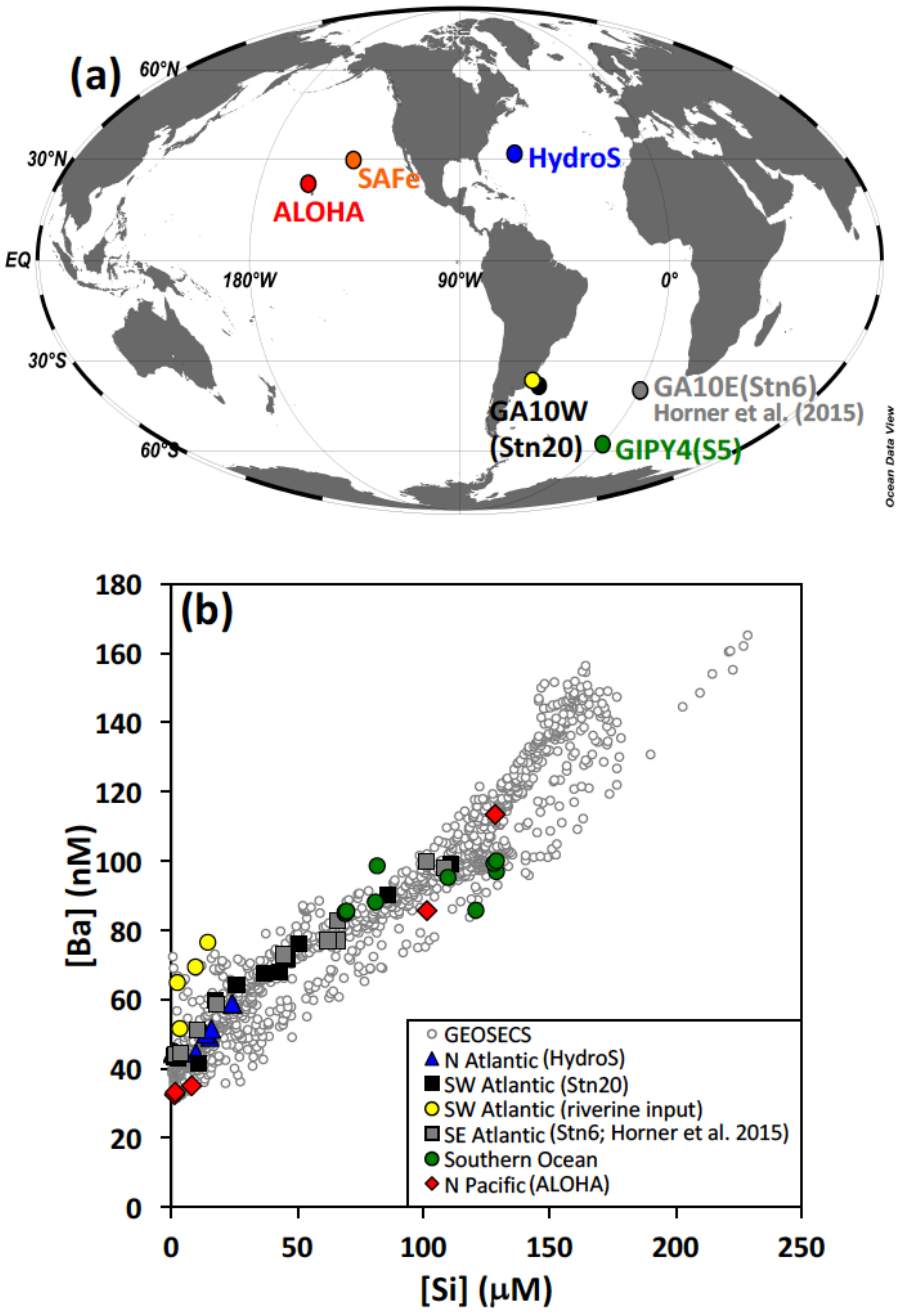

Figure 1 Map of sampling locations and the distribution of dissolved [Ba] and [Si] in global seawater. (a) The station symbols and data are colour coded consistently for each station throughout this paper. The data for GA10E (Stn6) are taken from Horner et al. (2015). (b) The yellow circles are samples that were collected along the GA10W cruise from Stn20 towards the Rio de la Plata in the SW Atlantic. Latitudes and longitudes are in Table 1. The [Ba] and [Si] concentrations from the GEOSECS Atlantic, Pacific and Southern Ocean dataset are shown in grey open circles (from https://odv.awi.de/en/data/ocean/geosecs/).

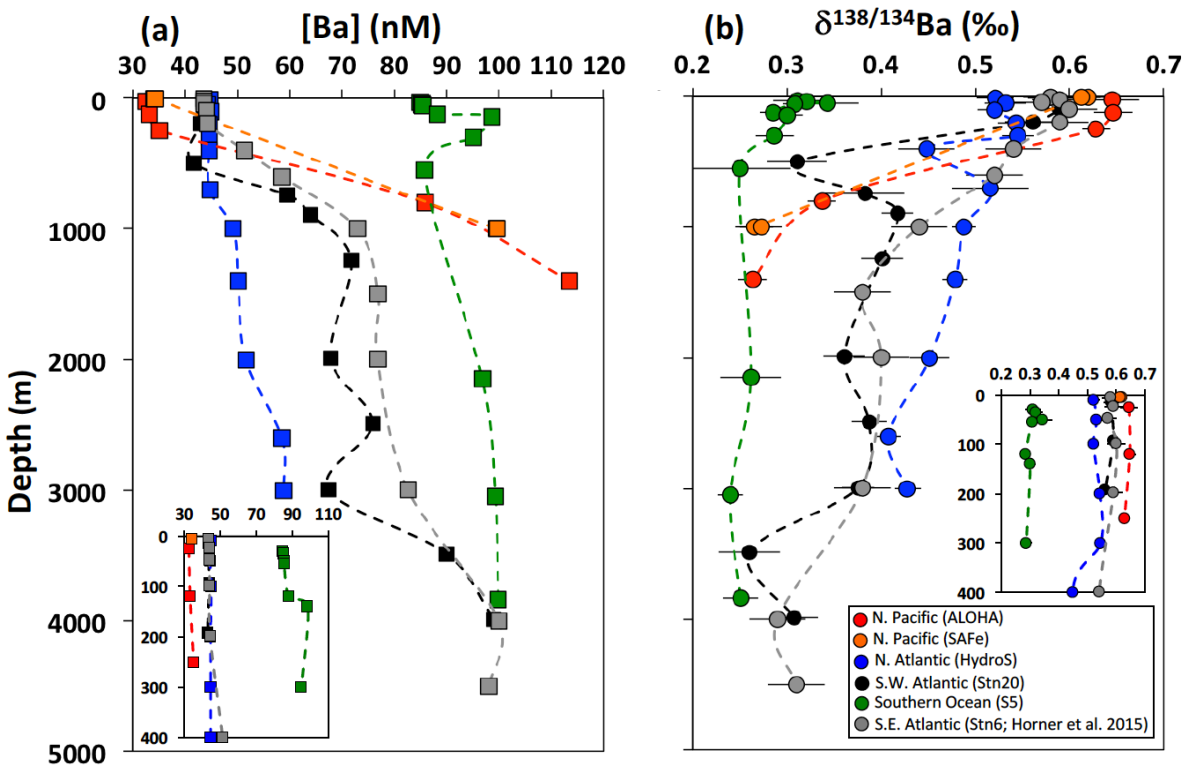

Figure 2 Depth profiles of **(a)** Ba concentrations and **(b)** Ba isotope compositions. The error bars of the data are 2 standard errors (2 S.E.), and are within the size of the symbols for [Ba]. The data for the SE Atlantic (Stn6) are taken from Horner et al. (2015).

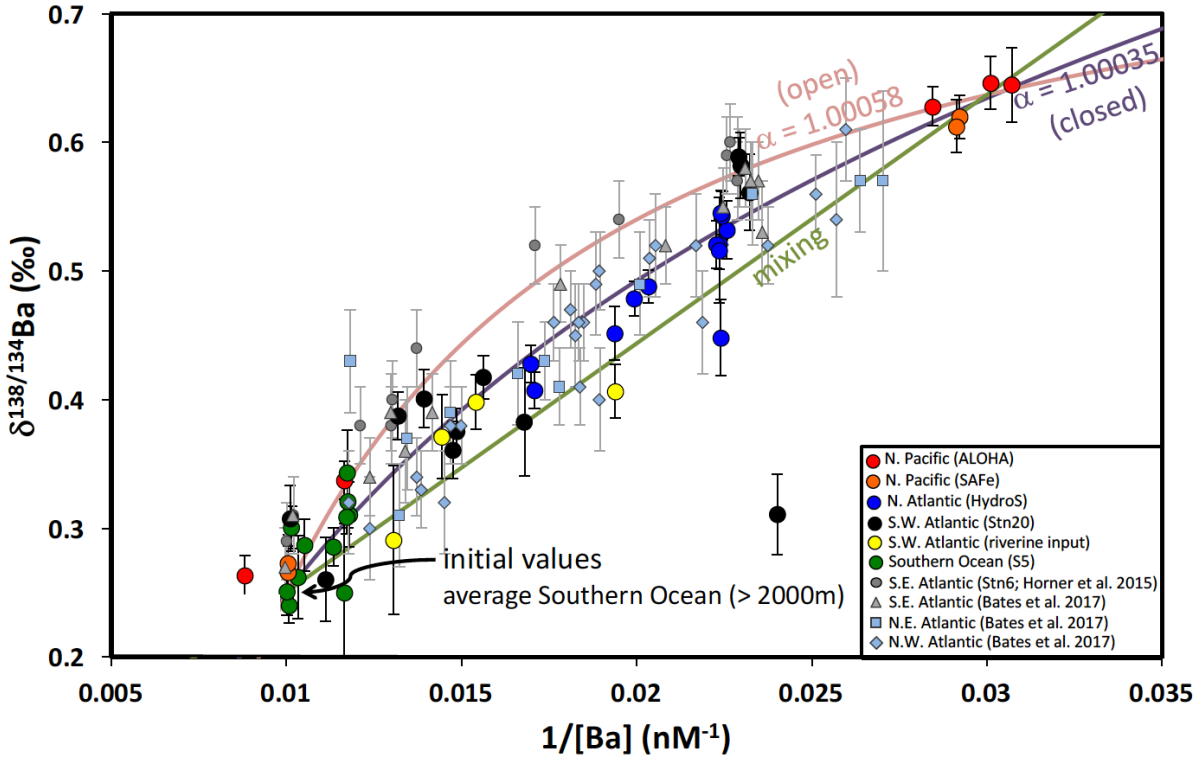

Figure 3 Ba isotope compositions versus 1/[Ba] for all seawater samples from this study, Horner et al. (2015) and Bates et al. (2017). The data are fitted with three curves generated by a steady-state (open) model, a Rayleigh fractionation (closed) model and a mixing model, each constrained using an initial composition equal to the average value in the deep Southern Ocean, and a final value equal to the surface values in the Pacific Ocean.

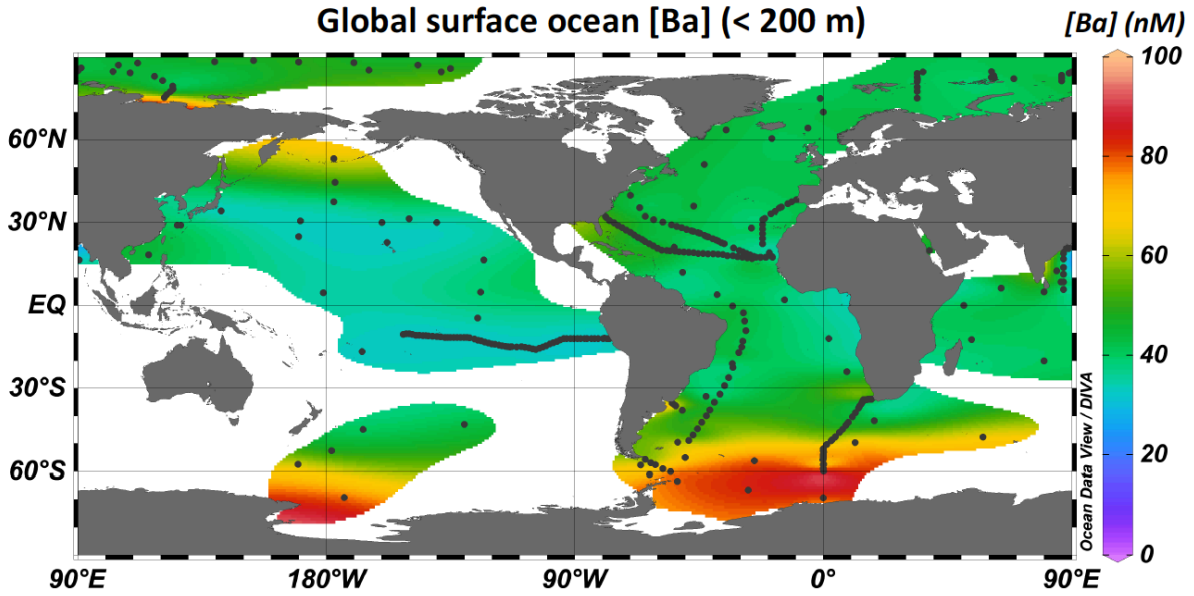

Figure 4 Global surface seawater [Ba] map (< 200m). Data sources are from the GEOSECS (Chan et al. 1976; Chan et al. 1977; Bacon and Edmond 1972), the GEOTRACES Intermediate Data Product 2014 (Cruises: GIPY4: Hoppema et al. 2010; GIPY5: data courtesy of T. Roeske and M. Rutgers van der Loeff; GIPY11: Roeske et al. 2012; GA02: data courtesy of A. Vilela and J.M. Godoy), and other GEOTRACES Cruises (GA03 and GP16 data courtesy of A. Shiller, and GA10: Horner et al. 2015 and this study) for the global oceans, and Singh et al. (2013) for Bay of Bengal, and Cao et al. (2016) for the South and East China Seas.

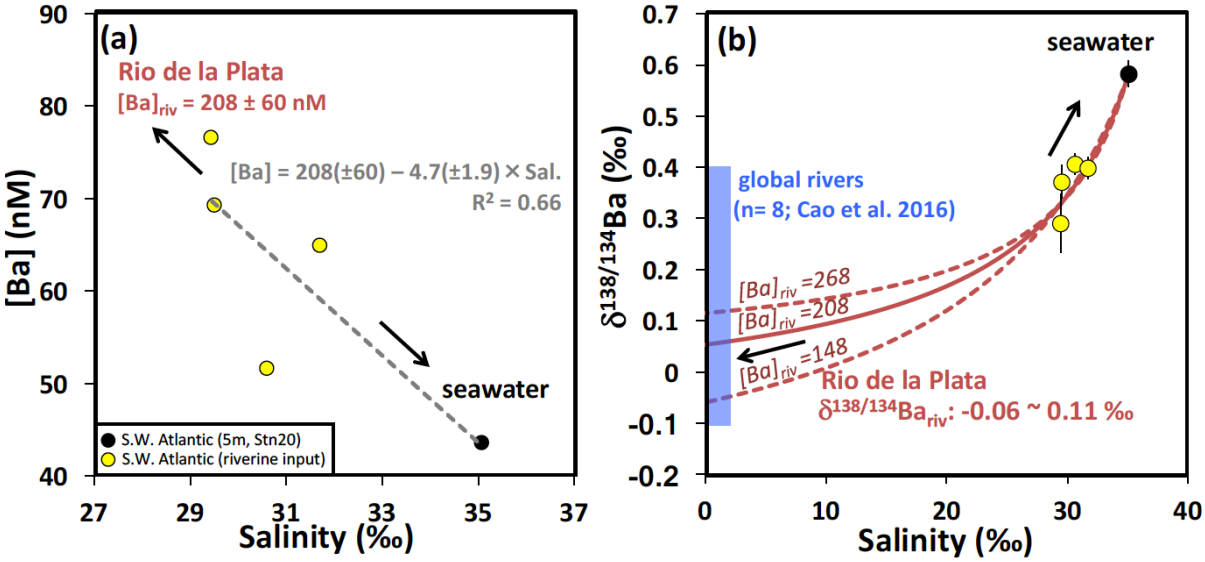

Figure 5 Ba concentrations and isotopic compositions in the surface samples with riverine input from the Rio de la Plata in the SW Atlantic. **(a)** Ba concentration versus salinity shows evidence for mixing between seawater and riverine input indicating a [Ba] = 208 ± 60 nM in the riverine input at salinity of 0 ‰. **(b)** Seawater $\delta^{138/134}$Ba versus salinity. The solid and dashed lines show the two end-member mixing curve between seawater (salinity at 35 ‰) and riverine input (salinity at 0 ‰) with a range of estimate of river [Ba] from 148 nM to 268 nM and predicted $\delta^{138/134}$Ba from -0.06 to 0.11 ‰. The range of observed global riverine $\delta^{138/134}$Ba from eight rivers is labeled in light blue (data from Cao et al. 2016).

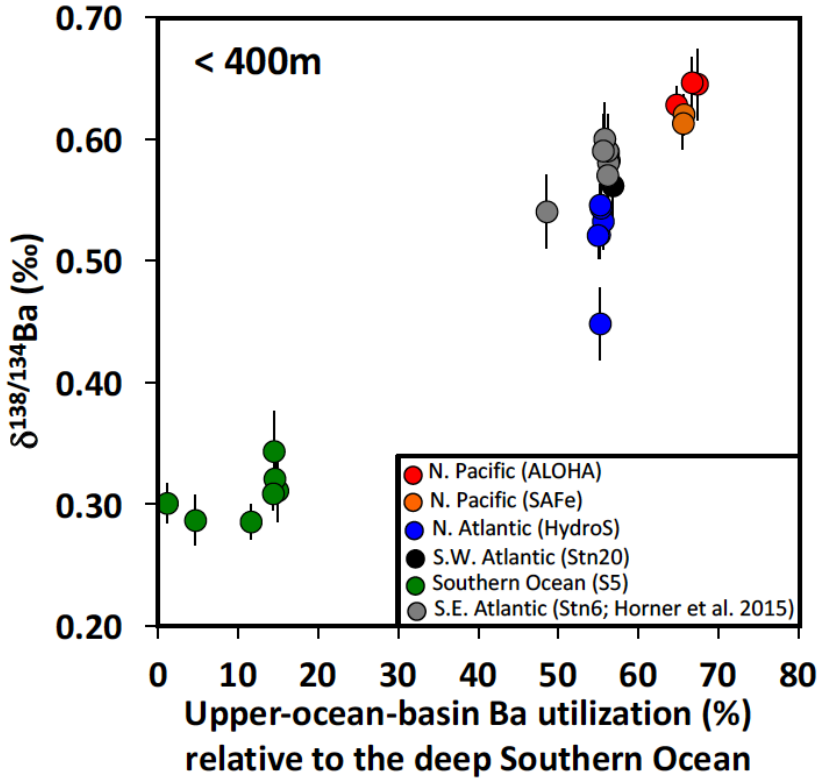

Figure 6 Seawater Ba isotopic compositions and the relative basin-scale Ba utilization relative to the composition of the deep Southern Ocean. The relative ocean-basin-scale Ba utilization is calculated by normalizing surface seawater [Ba] (< 400m) to the average [Ba] (99.7 nM) in the deep Southern Ocean (> 2000m).

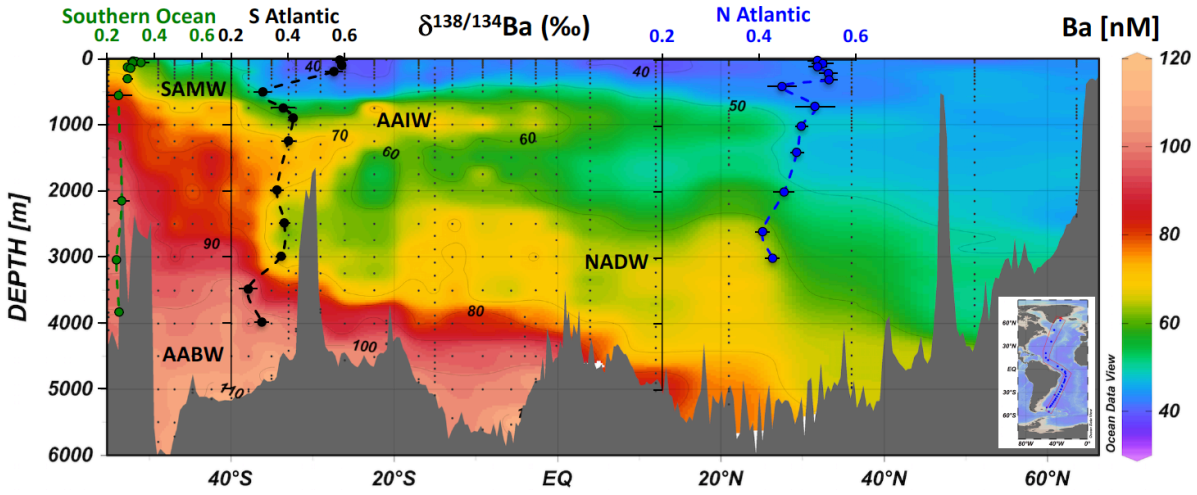

Figure 7 Seawater [Ba] and $\delta^{138/134}$Ba profiles in a N-S Atlantic section. The dissolved [Ba] data are from the GEOTRACES Intermediate Data Product 2014 (Mawji et al., 2015) and the GEOSECS Ba dataset (Fig. 1b). Seawater $\delta^{138/134}$Ba profiles are shown for the North Atlantic, South Atlantic and Southern Oceans (from this study).

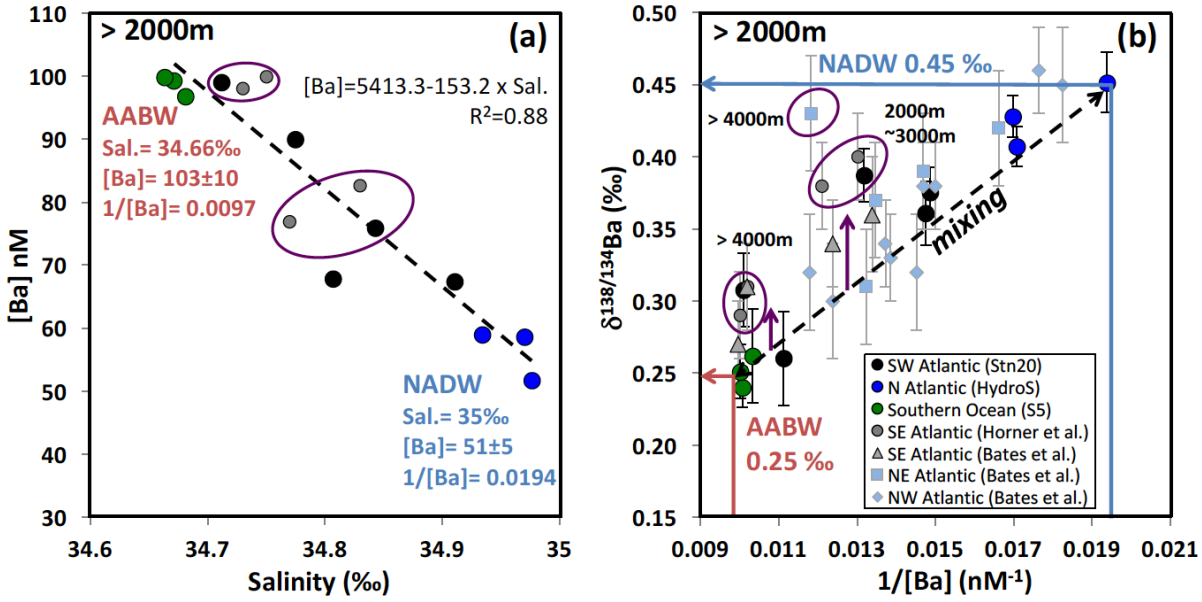

Figure 8 Seawater [Ba] and $\delta^{138/134}$Ba below 2000 m in the Atlantic. **(a)** The linear regression of [Ba] and salinity in the deep Atlantic Ocean; end-member salinity values are 35.00 and 34.66 ‰ in NADW and AABW respectively (Emery and Meincke, 1986), suggesting [Ba] of 51 ± 5 nM and 103 ± 10 nM in NADW and AABW respectively. **(b)** Deep-water $\delta^{138/134}$Ba versus 1/[Ba]. The end-member [Ba] concentrations in NADW and AABW are labeled with blue and red lines respectively, which indicate that NADW has a $\delta^{138/134}$Ba value of 0.45 ‰ and AABW has a $\delta^{138/134}$Ba value of 0.25 ‰. Deep-water $\delta^{138/134}$Ba and [Ba] in the South Atlantic show non-conservative mixing during the N-S Atlantic water transport as highlighted by purple arrows and circles. These deviations show $\delta^{138/134}$Ba offsets of 0.05 ~ 0.14 ‰ from the mixing line in deep waters. The SE Atlantic data (labeled in gray) and the NE and NW Atlantic data (labeled in light blue) are from Horner et al. (2015) and Bates et al. (2017).

Table 1 Seawater sample information, temperature, salinity, Ba concentration, and Ba isotope composition

Sampling site	Cruise	Station	Latitude	Longitude	Depth (m)	Temperature (^{o}C)	Salinity (PSU)	[Ba] (nM)	$\delta^{138/134}$Ba ($^{o}/_{oo}$) ±2SE
North Atlantic	61183	Hydrostation S	32.17	-64.50	11	27.91	36.67	44.7	0.52 ± 0.02
			32.17	-64.50	51	22.23	36.61	44.3	0.53 ± 0.02
			32.17	-64.50	100	19.41	36.66	44.9	0.52 ± 0.02
			32.17	-64.50	199	18.14	36.56	44.6	0.54 ± 0.02
			32.17	-64.50	301	17.76	36.52	44.6	0.55 ± 0.02
			32.17	-64.50	400	17.12	36.41	44.6	0.45 ± 0.03
			32.17	-64.50	701	11.87	35.53	44.7	0.52 ± 0.04
			32.17	-64.50	1000	6.69	35.11	49.2	0.49 ± 0.01
			32.17	-64.50	1400	4.90	35.07	50.2	0.48 ± 0.01
			32.17	-64.50	1999	3.67	34.98	51.6	0.45 ± 0.02
			32.17	-64.50	2600	3.23	34.97	58.5	0.41 ± 0.01
			32.17	-64.50	2998	2.80	34.93	58.9	0.43 ± 0.01
South Atlantic	GA10	STN20	-37.98	-51.03	14	21.50	35.08	43.5	0.58 ± 0.03
			-37.98	-51.03	93	17.10	35.63	43.6	0.59 ± 0.01
			-37.98	-51.03	192	13.50	35.33	43.1	0.56 ± 0.03
			-37.98	-51.03	498	6.65	34.38	41.6	0.31 ± 0.03
			-37.98	-51.03	741	4.44	34.21	59.6	0.38 ± 0.04
			-37.98	-51.03	890	3.74	34.22	64.0	0.42 ± 0.02
			-37.98	-51.03	1240	3.18	34.36	71.8	0.40 ± 0.02
			-37.98	-51.03	1988	3.37	34.81	67.8	0.36 ± 0.02
			-37.98	-51.03	2488	2.94	34.84	75.9	0.39 ± 0.02
			-37.98	-51.03	2993	2.84	34.91	67.3	0.38 ± 0.02
			-37.98	-51.03	3487	1.69	34.77	89.9	0.26 ± 0.03
			-37.98	-51.03	3988	0.94	34.71	99.0	0.31 ± 0.03
		Underway	-36.30	-53.41	5	23.06	29.44	76.5	0.29 ± 0.05
			-35.84	-54.18	5	22.98	29.51	69.3	0.37 ± 0.03
			-35.49	-54.56	5	23.04	30.61	51.6	0.41 ± 0.02
			-35.40	-54.66	5	22.57	31.71	64.9	0.40 ± 0.02
Southern Ocean	GIPY4	Super5	-57.55	0.04	30	0.42	34.24	84.8	0.31 ± 0.03
			-57.55	0.04	35	0.42	34.24	85.2	0.32 ± 0.02
			-57.55	0.04	50	0.40	34.09	85.3	0.34 ± 0.03
			-57.55	0.04	55	0.40	34.09	85.4	0.31 ± 0.01
			-57.55	0.04	120	-0.62	34.42	88.2	0.29 ± 0.01
			-57.55	0.04	140	-0.70	34.47	98.6	0.30 ± 0.02
			-57.55	0.04	300	0.44	34.65	95.1	0.29 ± 0.02
			-57.55	0.04	550	0.52	34.57	85.8	0.25 ± 0.05
			-57.55	0.04	2150	-0.13	34.68	96.8	0.26 ± 0.03
			-57.55	0.04	3050	-0.30	34.67	99.3	0.24 ± 0.01
			-57.55	0.04	3840	-0.37	34.66	99.8	0.25 ± 0.02
North Pacific	HOE-PhoR II	ALOHA	22.75	-158	25	26.82	35.49	32.6	0.64 ± 0.03
			22.75	-158	120	21.26	35.28	33.2	0.65 ± 0.02
			22.75	-158	249	14.50	34.42	35.2	0.63 ± 0.02
			22.75	-158	801	4.48	34.35	85.8	0.34 ± 0.02
			22.75	-158	1400	3.09	34.55	113.4	0.26 ± 0.02
	SAFe	SAFe	30	-140	20	19.23	34.75	34.2	0.62 ± 0.02
			30	-140	20	19.23	34.75	34.3	0.61 ± 0.02
			30	-140	1000	3.69	34.41	99.5	0.27 ± 0.02
			30	-140	1000	3.69	34.41	99.6	0.27 ± 0.02

Barium stable isotopes in the global ocean:

Tracer of Ba inputs and utilization

Supplementary material

Yu-Te Hsieh[a,*] and Gideon M. Henderson[a]

[a]University of Oxford, Department of Earth Sciences, South Parks Road, Oxford, OX1 3AN, UK

*Corresponding author: yu-te.hsieh@earth.ox.ac.uk

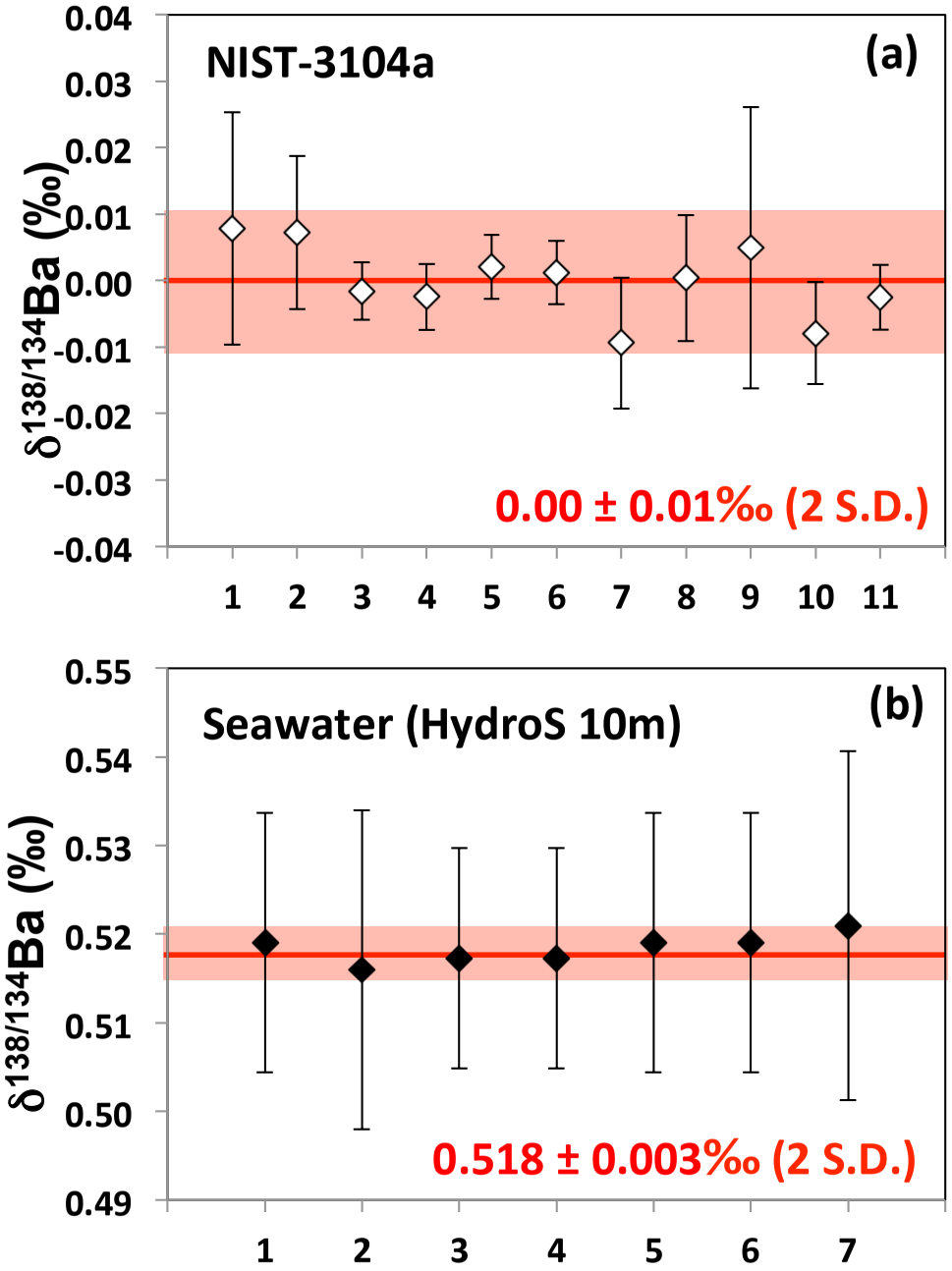

Figure S1. Replicated $\delta^{138/134}$Ba data of (a) NIST-3104a Ba standard, and (b) seawater sample from the HydroS station 10 m depth. The error bar of each data point presents the internal reproducibility, 2 standard errors (2 S.E., n = 500). The NIST data were collected over two years from September 2014 to September 2016 on the Triton TIMS at the University of Oxford. Seawater no.1 to no.6 were six of the same sample, and each one has been through independent chemistry. These samples were measured within one week in October 2015. Seawater no. 7 was the same sample as no.1 to no.6 but measured in June 2015. NIST measurements show an external reproducibility of 0.01 ‰ (2 standard deviations) over two years. However, seawater data show an external reproducibility of 0.003 ‰ (2 standard deviation), which is surprisingly good and even better than the NIST measurements. This could be due to the fact that seawater data were collected within a short period of time. Nevertheless, both datasets suggest that the instrument and seawater chemistry are relatively reliable and consistent for both long-term and short-term performances. As the internal errors of seawater samples are generally larger than the external errors, we therefore report the internal errors in this study.

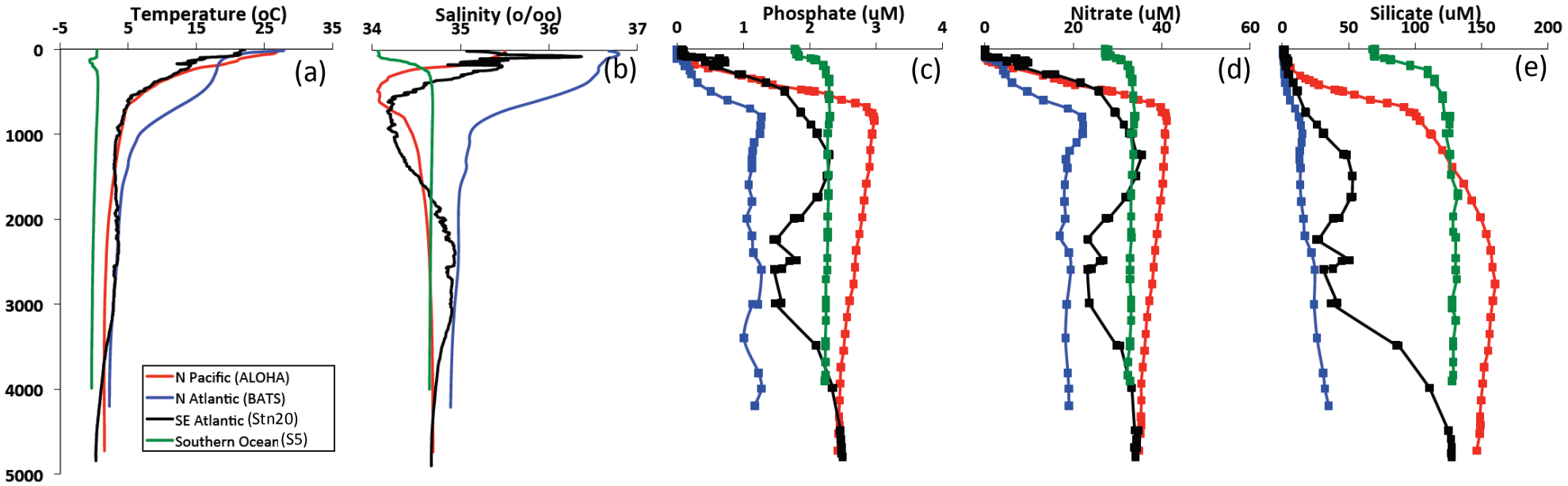

Figure S2. Data of (a) temperature, (b) salinity, (c) phosphate, (d) nitrate and (e) silicate at each station in North Pacific (ALOHA), North Atlantic (HydroS), South West Atlantic (Stn20) and Southern Ocean (S5).

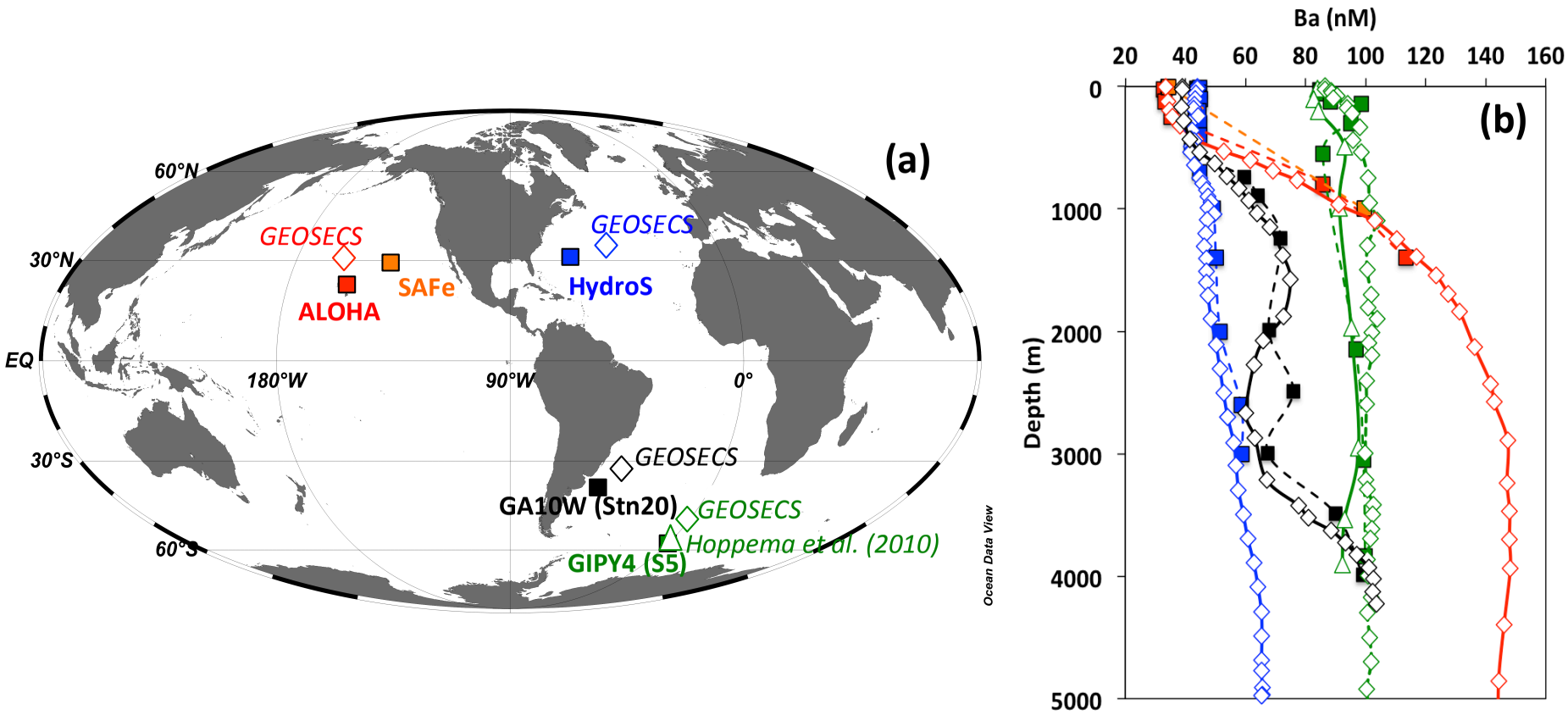

Figure S3. Comparison of seawater Ba concentrations from this study with the previous results from the GEOSECS (Chan et al., 1976, and Chan et al, 1977) and Hoppema et al. (2010).

Table S1 Ba standard and double spike isotope calibrations

	137Ba/138Ba ±2SE	**135Ba/138Ba ±2SE**	**134Ba/138Ba ±2SE**	
NIST3104a	0.1565372 ± 0.0000003	0.0919451 ± 0.0000003	0.0337176 ± 0.0000002	(n=8)
137Ba-135Ba double spike	3.301030 ± 0.000006	8.22360 ± 0.00005	0.0423760 ± 0.0000003	(n=11)

The Ba standard and the 137Ba-135Ba double spike calibrations were measured on TIMS. For the Ba standard NIST3104a, the Ba isotope compositions were normalized to $^{138}Ba/^{136}Ba = 9.12875$ (Ranen and Jacobsen, 2006) following the exponential law for the instrument mass fractionation. The double spike calibration was measured in 11 independent mixtures of spike and standard.

Text S1. Ba double spike deconvolution

The Ba isotope composition of samples and standards was determined by the double spike technique that has been widely used in different isotope systems. In this study, we used a ^{137}Ba-^{135}Ba double spike, and assumed that the mass fractionation follows an exponential law. The deconvolution equations can be described as:

$$F^{137}\{^{138}P_{spk}, B_{samp}, B_{mix}\} = {}^{138}P_{spk} \times ({}^{137}Ba/{}^{138}Ba)_{spk\text{-}t} + (1- {}^{138}P_{spk}) \times ({}^{137}Ba/{}^{138}Ba)_{samp\text{-}m} \times (M_{137}/M_{138})^{Bsamp} - ({}^{137}Ba/{}^{138}Ba)_{mix\text{-}m} \times (M_{137}/M_{138})^{Bmix} = 0$$

$$F^{135}\{^{138}P_{spk}, B_{samp}, B_{mix}\} = {}^{138}P_{spk} \times ({}^{135}Ba/{}^{138}Ba)_{spk\text{-}t} + (1- {}^{138}P_{spk}) \times ({}^{135}Ba/{}^{138}Ba)_{samp\text{-}m} \times (M_{135}/M_{138})^{Bsamp} - ({}^{135}Ba/{}^{138}Ba)_{mix\text{-}m} \times (M_{135}/M_{138})^{Bmix} = 0$$

$$F^{134}\{^{138}P_{spk}, B_{samp}, B_{mix}\} = {}^{138}P_{spk} \times ({}^{134}Ba/{}^{138}Ba)_{spk\text{-}t} + (1- {}^{138}P_{spk}) \times ({}^{134}Ba/{}^{138}Ba)_{samp\text{-}m} \times (M_{134}/M_{138})^{Bsamp} - ({}^{134}Ba/{}^{138}Ba)_{mix\text{-}m} \times (M_{134}/M_{138})^{Bmix} = 0$$

where $^{138}P_{spk}$ is the proportion of ^{138}Ba from the spike to the total ^{138}Ba in the mixture ($^{138}Ba_{spk}/^{138}Ba_{mix}$); B_{samp} and B_{mix} are the mass fractionation factors in the nature sample and in the spike-sample mixture respectively. The isotope ratios labeled with spk-t, samp-m, and mix-m stand for spike true, sample measured, and mixture measured ratios respectively. M_{138}, M_{137}, M_{135}, and M_{134} are the masses of referred Ba isotope. The equations were solved by converging the Newton-Raphson steps until the three spike-sample mixture functions F^{137},F^{135} and F^{134} were zero. We modified an Excel spreadsheet used in Bonnand et al. (2011) with the macro to do the iteration.

References

Bonnand, P., Parkinson, I.J., James, R.H., Karjalainen, A.-M., Fehr, M.A., 2011. Accurate and precise determination of stable Cr isotope compositions in carbonates by double spike MC-ICP-MS, J. Anal. At. Spectrom. 26, 528–535. doi: 10.1039/C0JA00167H

Chan, L.H., Edmond, J.M., Stallard, R.F., Broecker, W.S., Chung, Y.C., Weiss, R.F., Ku, T.L., 1976. Radium and barium at GEOSECS stations in the Atlantic and Pacific. Earth Planet. Sci. Lett. 32, 258-267. doi:10.1016/0012-821X(76)90066-2

Chan, L.H., Drummond, D., Edmond, J.M., Grant, B., 1977. On the barium data from the Atlantic GEOSECS expedition. Deep-Sea Res. 24, 613-649. doi:10.1016/0146-6291(77)90505-7

Hoppema, M., Dehairs, F., Navez, J., Monnin, C., Jeandel, C., Fahrbach, E., de Baar, H.J.W., 2010. Distribution of barium in the Weddell Gyre: Impact of circulation and biogeochemical processes. Mar. Chem. 122, 118-129. doi:10.1016/j.marchem.2010.07.005

Ranen, M.C., Jacobsen, S.B., 2006. Barium isotopes in chondritic meteorites: implications for planetary reservoir models. Science 314, 809-812. doi: 10.1126/science.1132595